Part I
Synthetic Methods

New Strategies in Chemical Synthesis and Catalysis, First Edition. Edited by Bruno Pignataro.

1
Electrospray and Cryospray Mass Spectrometry: From Serendipity to Designed Synthesis of Supramolecular Coordination and Polyoxometalate Clusters

Haralampos N. Miras and Leroy Cronin

1.1
Introduction

Molecular self-assembly is an exciting occurrence which governs how simple building blocks [1] can be organized spontaneously into complex architectures [2]. Such self-assembly processes are highly dependent upon the experimental conditions [3] often to such a degree that total control is never easily achieved [4]. This can be frustrating since extremely small changes in reaction conditions can yield totally different results [5]. For instance, many research groups have reported the discovery of new building blocks, architectures, and materials that exhibit fundamentally new and interesting properties as a result of the self-assembly process that were simply not expected [6]. The serendipitous result in self-assembled chemical systems usually lacks the element of design. On the other hand, little progress would be made if serendipity (i.e., chance discoveries) was the only guide [7]. Future work usually uses valuable information that is extracted by observations made from earlier studies and used as a starting point for a more designed approach. Representative examples that fall into the category of self-assembled chemical systems are the polynuclear coordination compounds and the polyoxometalate (POM) clusters.

POM clusters represent an unparalleled range of architectures and chemical properties, acting as a set of transferable building blocks that can be reliably utilized in the formation of new materials. These key features are being exploited rapidly today after a rise in popularity of POMs over the last two decades [8, 9]. Today, POM chemistry is an important, emerging area that promises to allow the development of sophisticated molecule-based materials and devices with numerous applications ranging from electronics and catalysis to physics [10–13]. The reason for the explosion in the number of structurally characterized POM compounds is due to developments in instrumentation and novel synthetic approaches. In terms of technique development, fast and routine single-crystal data collection has allowed the area to accelerate to the point where the bottle neck has moved to structure refinement and crystallization of new compounds rather than the time taken for data collection and initial structure solution. However, despite all the promise, the

New Strategies in Chemical Synthesis and Catalysis, First Edition. Edited by Bruno Pignataro.

relentless increase in the number of structures and derivatives mean that it can be difficult to distinguish between the different cluster types and subtypes, whereas till now it seemed hard to be sure that the processes that govern the self-assembly of these complex architectural systems can be fully controlled and directed.

In a similar manner, supramolecular chemistry has been described by researchers as an information science in which libraries of building blocks that contain the necessary information self-assemble into larger architectures [14]. Complementary and precise interaction of individual species with the appropriate symmetry, geometry, and chemical information directs the product assembly. Also in this case, there is a long list of variables that triggers and directs the whole process by creating an experimental environment in which the ''fittest'' species prevail and evolve into the final product following the most energetically favorable route. Consequently, self-assembly has been recognized as a powerful tool for the construction of supramolecular scaffolds, as demonstrated by a plethora of exciting contributions [15].

The development of both classes of materials and exploitation of their potential require the ability to design novel synthetic procedures and the capacity to use results obtained by serendipity constructively in order to maximize the desirable outcome and the understanding of the selection rules that govern these chemical systems. In both the aforementioned cases, it is a great challenge and extremely important to understand and control the self-assembly. During this effort, the conventional spectroscopic techniques present significant drawbacks. For example, nuclear magnetic resonance (NMR) is of limited use when the symmetry of the assembled architecture is high [16], when the structures are labile or paramagnetic, and when the nuclei have poor receptivity. Additionally, the reaction mixtures are far too complicated to extract any useful information regarding the nature and availability of the building-block libraries, the selection rules that trigger their organization in a controlled fashion, as well as the preferable pathway that is selected for the formation of the polynuclear clusters.

Therefore, given the enormous challenge in understanding and controling the self-assembly process for a range of self-assembled, cluster-based architectures, high-resolution time-of-flight mass spectrometry (TOF-MS) has been employed over the last decade in an effort to shine light upon the assembly–disassembly process of high-nuclearity POMs and coordination clusters as well to identify novel reactive and intermediate species in reaction mixtures. Herein, we discuss the most recent developments and how electrospray ionization mass spectrometry (ESI-MS), cryospray ionization mass spectroscopy (CSI-MS), and variable temperature mass spectrometry (VT-MS) with a high-resolution TOF detector could offer a novel approach in overcoming the present difficulties, revealing important mechanistic information and allowing the identification of the building-block libraries present in solution under specific experimental conditions. Furthermore, this will allow us to take real control over the self-assembly processes and open the door for further exploration, discoveries, and, ultimately, well-established designing methodologies toward materials with predefined functionalities.

1.2 Background to ESI-MS

ESI-MS has been used extensively to investigate many types of POMs including vanadates [17], niobates [18], tantalates [19], chromates [20], molybdates [21], tungstates [22–24], and rhenates [25]. Howarth *et al.* investigated aqueous solutions of isopolytungstates, peroxotungstates, and heteropoly-molybdates, detecting the $[W_6O_{19}]^{2-}$ and $[W_2O_7]^{2-}$ species in aqueous solution for the first time [26]. Mixed-metal heteropolyanion clusters were also investigated, and the series of $[H_xPW_nMo_{12-n}O_{40}]^{(3-x)-}$ species reported. Further, it was shown that the ESI-MS-determined concentration of sensitive species (i.e., sensitive to changes in pH or the presence of other species) may differ from that determined in bulk measurements. Such studies have been extended to other clusters. For instance, it was shown that heteropolyoxomolybdate [27] compounds in acetonitrile could be successfully identified as intact anionic species, for example, $[S_2Mo_{18}O_{62}]^{2-}$. Also, mixed-metal polyoxomolybates and tungstates could be identified in solution [28], and studies on isopolyoxomolybdates [21], tungstates [22–24], and even isopolyoxochromates [20] have been reported. In each case, an aggregation process of additive polymerization involving $\{MoO_3\}$, $\{WO_3\}$, or $\{CrO_3\}$ moieties, respectively, was identified as giving rise to the larger POM aggregates observed. In addition, the wide applicability of the ESI-MS technique to complex systems and mixtures has been demonstrated in catalytic studies, where the real-time transformation of the substrate could be observed, helping the proposal of a mechanistic pathway [29a,b]. Studies of the potential-dependent formation of unknown multinuclear and mixed-valence polyoxomolybdate complexes when using online electrochemical flow cell electrospray mass spectrometry (EC-ESI-MS) have also been presented [29c].

1.2.1 Background to CSI-MS

CSI-MS was developed by Yamaguchi *et al.* [30] in order to investigate unstable organometallic complexes in which the presence of weak noncovalent interactions had precluded analysis by other ionization techniques such as fast-atom bombardment (FAB), matrix-assisted laser desorption ionization (MALDI), and ESI because of dissociation of the species. The technique is, therefore, of interest for investigations of labile POM systems because previous ESI-MS studies of such systems have been limited by the use of low-resolution detectors and the high temperatures utilized in the ESI process. The cryospray apparatus consists of, essentially, an electrospray source where the N_2 capillary and sprayer gases are maintained at very low temperatures ($\sim -100\,^{\circ}C$). The use of low-temperature gases promotes ionization of the target molecules, not by desolvation as in the conventional ESI process, but by increasing the polarizability of the target molecules at low temperature (i.e., the result of higher dielectric constant at low temperature). This allows the molecular ions of unstable species to be generated and transferred efficiently into the MS

detector with minimal fragmentation effects [30]. An example of the potential of CSI-MS to investigate weakly hydrogen-bonded organic aggregates is the observation of large hydrogen-bonded chain structures of amino acids in solution, for example, L-serine, glycine, L-valine [31]. These observations are consistent with the single-crystal X-ray crystallographic data for some of these amino acids in the solid state. Furthermore, the use of CSI-MS studies in more complicated molecules of biological interest was crucial in an effort to investigate the conformational changes of human telomerase upon binding with naphthyridine dimmers [32]. The application of CSI-MS analysis to Pd and Pt cages and their host–guest chemistry has been successful as well as a result of the mild experimental conditions (low temperature). The use of NMR proved not to be very informative since it is difficult to determine precisely the number and structures of the guest molecules if plural guest molecules are encapsulated within the cage compound, whereas during the ESI-MS studies extensive fragmentation takes place because the majority of the Pt/Pd cages are unstable at the temperatures (100 °C) of the desolvation plate. Investigation of the constitution of Grignard reagents [33] in solution is extremely challenging. The use of CSI-MS studies, though, allowed the identification of the species in solution, which supports the idea that the major species of RMgCl Grignard-type reagents in tetrahydrofuran (THF) has the formula $RMg_2(\mu\text{-}Cl_3)$ [33]. CSI-MS is also applicable to the investigation of labile solution structures of various biomolecules. In the case of DNA, for example, various complexes of oligodeoxynucleotides were identified, and it was possible to observe very unstable species such as low-melting-temperature DNA duplexes which could not be detected by the conventional ESI-MS technique [34].

1.3 Application of High-Resolution ESI-MS and CSI-MS to Polyoxometalate Cluster Systems

In the context of this chapter, it is worth pointing out that POMs are ideal candidates for high-resolution studies since they have complex isotopic envelopes resulting from the high number of stable isotopes of tungsten (^{182}W, 26.5%; ^{183}W, 14.3%; ^{184}W, 30.6%; and ^{186}W, 28.4%) and molybdenum (^{92}Mo, 14.8%; ^{94}Mo, 9.3%; ^{95}Mo, 15.9%; ^{96}Mo, 16.7%; ^{97}Mo, 9.6%; ^{98}Mo, 24.1%; and ^{100}Mo, 9.6%), and are intrinsically charged. This allows complete determination of the cluster formula down to the last proton by matching the calculated versus experimentally obtained distribution envelopes. The difficulty associated with determining the protonation state of the cluster has thus far been a major drawback of standard crystallographic X-ray diffraction (XRD) studies, which often do not provide direct information on the protonation state of the cluster anions. Therefore, MS of POMs has the potential to become the standard analysis technique for complex cluster systems since it provides vital complementary information of the cluster composition in solution that cannot be deduced from crystallographic studies, as shown by the following examples.

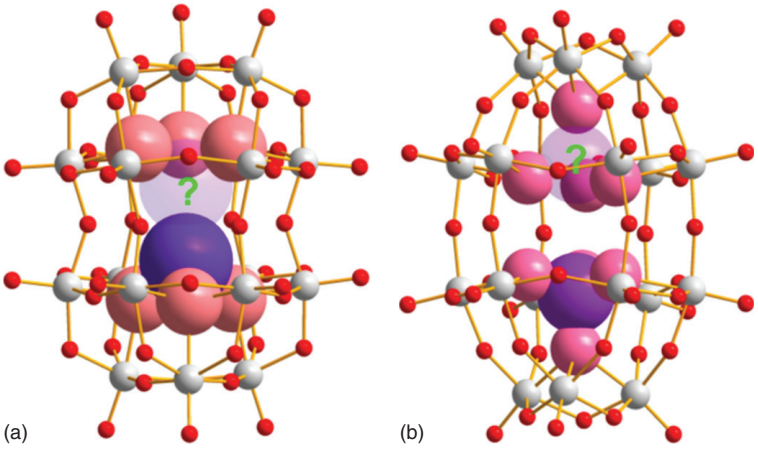

Figure 1.1 (a,b) Representation of the structures of $[H_mSb_nW_{18}O_{60}]^{y-}$ and $[H_mP_nW_{18}O_{62}]^{y-}$. Color scheme: W, gray; O, red; and Sb and P, purple.

1.3.1
Probing Protonation Versus Heteroatom Inclusion with ESI

The rugby-ball-shaped clusters [35] $[H_mW_{18}O_{60}X_n]^{y-}$ (where X = As, Sb, and Bi)[1)] have been known for three decades, with an approximate formulation of $n = 1$, but their precise composition could not be confirmed unambiguously because of disorder of the heteroatoms over two positions in a single cluster. However, by using ESI-MS, we recently reported the direct probing of the D_{3d} symmetric isomer of the Sb-based heteropolyoxotungstate $[H_mSb_nW_{18}O_{60}]^{y-}$ [13c]. During the course of these studies, we discovered that the correct formulation is one in which the cluster contains one hetero-ion disordered over two positions (Figure 1.1a). This situation can be compared with the discovery of $[H_mP_nW_{18}O_{62}]^{y-}$, which was also reported with $n = 1$ (see Figure 1.1b). Both clusters appear to include only one heteroatom; in addition, the $[H_4SbW_{18}O_{60}]^{7-}$ is templated by a pyramidal SbO_3^{3-} anion, whereas $[H_4PW_{18}O_{62}]^{7-}$ contains one tetrahedral PO_4^{3-} anion. ESI-MS results were obtained on tetrabutylammonium (TBM) salts of the clusters in acetonitrile solution (see Figures 1.2 and 1.3).

The cation exchange process was used because the TBA^+ cations have a much higher mass than Na^+ or K^+ and give a larger separation between signals corresponding to differently charged or protonated cluster states while at the

1) It should be noted that, when using both the techniques of ESI-MS and CSI-MS, the determined concentration of sensitive species (i.e., sensitive to changes in pH or the presence of other species) can still differ to some extent from that determined in bulk measurements. This effect was investigated by Howarth *et al.* during ESI-MS studies [26], and is due to the interference in the equilibrium process by the drying agent (e.g., nitrogen gas) as the desolvation rapidly affects the pH and the concentrations of the solutes in the formation of the analytes.

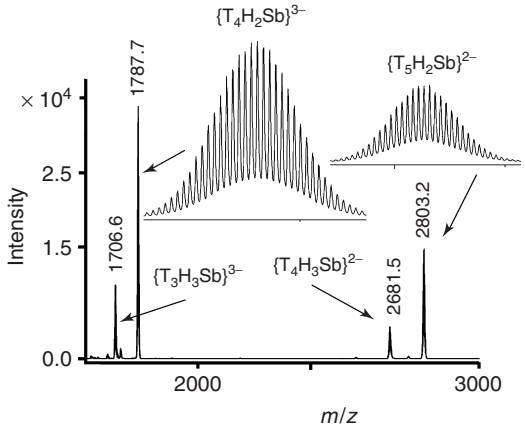

Figure 1.2 The negative ion mass spectrum of $[H_mSb_nW_{18}O_{60}]^{y-}$ showing the series of tri- and tetra-protonated forms of $(TBA)_y[H_xSb_1W_{18}O_{62}]^{(9-(x+y))-}$ in solution ($T = TBA^+$, $Sb = Sb_1W_{18}O_{60}$).

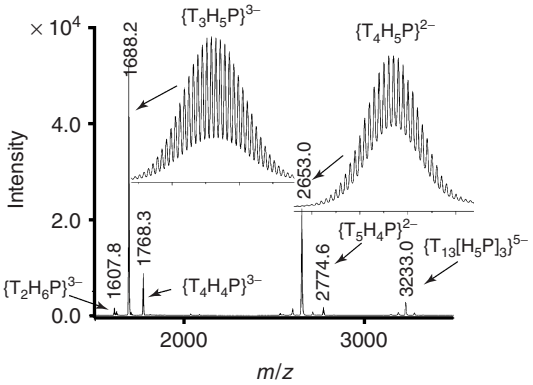

Figure 1.3 The negative ion mass spectrum of $[H_mP_nW_{18}O_{62}]^{y-}$ showing the series of tetra-, penta-, and hexa-protonated forms of $(TBA)_y[H_xP_1W_{18}O_{62}]^{(11-(x+y))-}$ in solution ($T = TBA^+$, $P = P_1W_{18}O_{62}$).

same time avoiding multiple overlapping distribution envelopes arising from different extents of protonation and/or hydration. Exhaustive analysis of the ESI-MS data shows that the compounds can be unambiguously identified in both positive and negative ion modes, and that the $[H_mSb_nW_{18}O_{60}]^{y-}$ species in solution to give the di- and tri-protonated forms (Figure 1.2) whereas $[H_mP_nW_{18}O_{62}]^{y-}$ can be observed as the hexa-, penta-, and tetra-protonated forms (Figure 1.3).

This study shows that heteropolyoxometalate clusters exist in solution in a range of accessible protonation states that can often not be identified by bulk analytical methods. For both compounds, the most intense single-ion signal or base peak

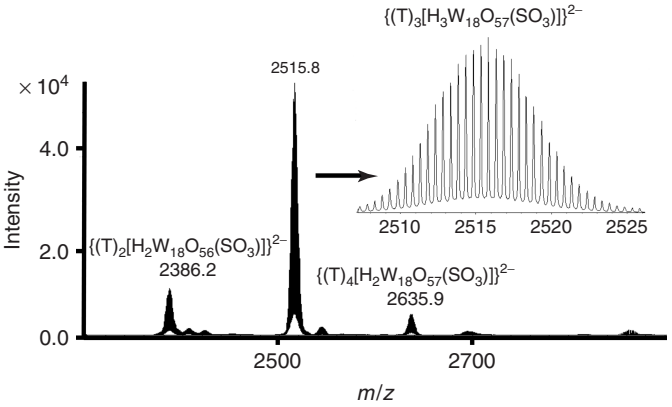

Figure 1.4 Negative ion mode mass spectra of $(TBA)_5[H_3W_{18}O_{57}(SO_3)]$ in acetonitrile ($T = TBA^+$).

was observed for the di- and penta-protonated species, respectively, and shows that it is possible to observe the protonation of a heteropoly acid as a function of the number of hetero-anions included within the cluster.

Also, using this data, it is possible to assign the protonation state of the cluster in the solid state. Furthermore, using a range of mixed-cluster ESI-MS experiments carried out as a function of concentration, we were able to quantify the transmitted ion intensity directly with the concentration of the cluster species in solution. This was done by comparison of the bis-phosphate Dawson cluster $(TBA)_6[P_2W_{18}O_{62}]$ with the monophosphate $(TBA)_6[H_5PW_{18}O_{62}]$. This gave a linear relationship between the relative ion intensity and the ratio of the concentration of the two compounds in solution. This means that in organic solvents it is possible to use ESI-MS studies to directly probe the solution equilibria.

In a similar manner, we recently reported the solution studies of the mono- and bi-sulfite tungsten-based capsules. The ESI-MS study of the monosulfite species in acetonitrile shows that the expected $\{W_{18}S\}$ cluster anion can be assigned unambiguously to different charge/cation states of this: *m/z* 2515.8 $\{(TBA)_3[H_3W_{18}SO_{60}]\}^{2-}$, 3434.8 $\{(TBA)_7[H_3W_{18}SO_{60}]_2\}^{3-}$, and 3001.4 $\{(TBA)_7[H_3W_{18}SO_{60}]\}^{2+}$ (see Figure 1.4 for the spectrum including an expansion of the main peak in the negative mode). The ESI-MS spectrum of the TBA salt of $\{W_{18}S\}$ clearly shows that the cluster is threefold protonated compared to the doubly protonated species found in its sodium analog; however, the composition of the main framework is otherwise identical as expected. It is interesting also to observe that the cluster is labile and that the parent threefold protonated cluster can decompose via water loss, as indicated by the peak at *m/z* 2386.2; this can be assigned to the $\{(TBA)_2[H_2W_{18}O_{56}(SO_3)]\}^{2-}$ species, which indicates that the decomposition process of the threefold protonated cluster may begin with the loss of one water molecule.

In contrast, the ESI-MS spectra of the bisulfite cluster anion in acetonitrile solvent are also recorded, and the expanded main peak is represented in

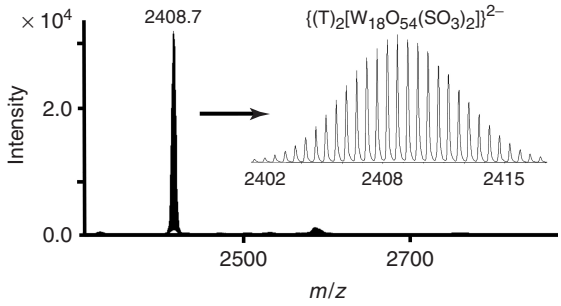

Figure 1.5 Negative ion mode mass spectra of $(TBA)_4[W_{18}O_{54}(SO_3)_2]$ in acetonitrile ($T = TBA^+$).

Figure 1.5, which gives totally different results. As reported previously [36], the $[W_{18}O_{56}(SO_3)_2(H_2O)_2]^{8-}$ cluster rearranges during the cation exchange process and forms the $[W_{18}O_{54}(SO_3)_2]^{4-}$ cluster. All the main peaks can be assigned, and related to the $\{W_{18}S_2\}$ species.

1.3.2
Solution Identification of Functionalized POMs

The functionalization of POM clusters via covalent grafting of organic functions allows the properties of the cluster to be tuned and novel functionalities to be introduced. In our recent work, an asymmetric, functionalized Mn-Anderson cluster was designed and synthesized, $(TBA)_3[MnMo_6O_{18}(C_4H_6O_3NO_2)(C_4H_6O_3NH_2)]$ [37], utilizing ESI-MS during the screening process of the reaction mixtures and fine adjustment of the experimental conditions of this labile system. Subsequently, the system was set up for crystallization, and the crystalline fractions were isolated from the mother liquor by filtration every 6 h. Each batch of the crystalline samples was then analyzed again using ESI-MS in order to determine the distribution and number of products present, allowing the correct batch to be ''sorted'' from the bulk, statistically defined mixture. The batch corresponding to the asymmetric compound was collected. Using this approach, ESI-MS studies not only helped the reaction mixtures to be ''sorted'' but also allowed confirmation of the intrinsic composition, as shown in Figure 1.6, and isolation of the pure crystalline phase of the desirable product. The peak at $m/z = 1669$ can be clearly assigned to the $[(TBA)_2\{MnMo_6O_{18}(C_4H_6O_3NO_2)(C_4H_6O_3NH_2)\}]^-$ anion. Additionally, the signal at $m/z = 1669$ is the only peak in the range of m/z 1300–2000, with no peaks being observed that would be expected from co-crystallization of the other possible species $[(TBA)_2\{MnMo_6O_{18}(C_4H_6O_3NH_2)_2\}]^-$ (m/z 1640) or $[(TBA)_2\{MnMo_6O_{18}(C_4H_6O_3NO_2)_2\}]^-$ (m/z 1700). The observation of such complex reaction mixtures under electrospray conditions is very important in the effort toward the design and synthesis of hybrid POM-based materials that possess the desirable functionality.

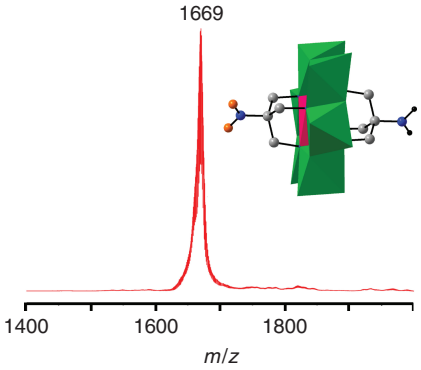

Figure 1.6 ESI-MS spectrum of the asymmetric compound in MeCN showing one signal at $m/z = 1669$ due to $[(TBA)_2\{MnMo_6O_{18}(C_4H_6O_3NO_2)(C_4H_6O_3NH_2)\}]^-$ species. Inset: representation of the X-ray crystal structure of $\{MnMo_6O_{18}(C_4H_6O_3NO_2)(C_4H_6O_3NH_2)\}^{2-}$. Color scheme: Mo, green polyhedra; Mn, pink polyhedron; C, gray; N, blue; O, orange; and H, black.

1.3.3
Solution Identification of New Isopolyoxotungstates and Isopolyoxoniobates

In our recent work, we targeted the exploration of aqueous solutions of isopolyoxotungstates using a combination of pH, ionic strength, and anion control to unravel the influence of these factors on the self-assembly of anionic isopolyoxotungstates. As such, we were able to demonstrate that it is possible to discover radically new cluster architectures in the isopolyoxotungstate family simply by acidifying solutions of sodium tungstate leading to the isolation and crystallization of an "S"-shaped $[H_4W_{22}O_{74}]^{12-}$ cluster (Figure 1.7) [12b].

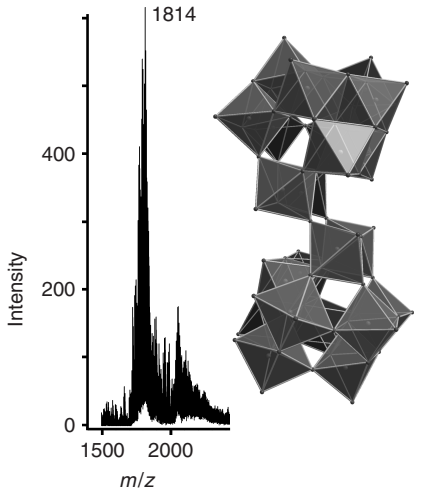

Figure 1.7 The crystal structure of the "S"-shaped cluster (b) and the negative ion mass spectrum for $\{(Na_9)[H_4W_{22}O_{74}]\}^{3-}$ in water (a). Simulation of the expected spectrum matches that of the observed peak at m/z 1814 [12b]. Color scheme: W, dark grey polyhedra and O, dark grey spheres.

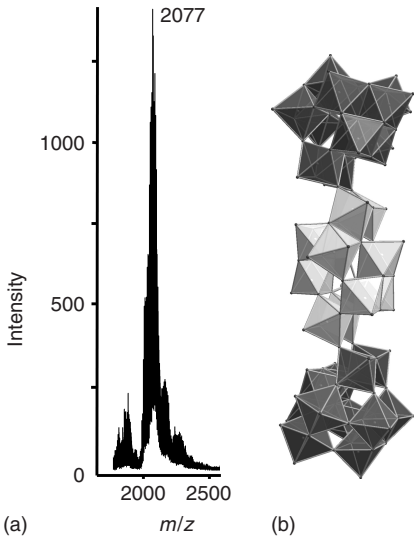

Figure 1.8 The crystal structure of the "∫"-shaped cluster (b) and the negative ion mass spectrum for $\{Na_8H_6[H_{10}W_{34}O_{116}]\}^{4-}$ in water (a). Simulation of the expected spectrum matches that of the observed peak at *m/z* 2077 [12b]. Color scheme: W_{22} unit, dark grey polyhedra; W_{34} unit, light grey polyhedra; and O, dark grey spheres.

The compound $Na_{12}[H_4W_{22}O_{74}] \cdot 31H_2O$ could not only be identified as containing the $[H_4W_{22}O_{74}]^{12-}$ anion in the solid state, but it was also identified in aqueous solution using ESI-MS analysis as the $\{(Na_9)[H_4W_{22}O_{74}]\}^{3-}$ anion at *m/z* 1814. The cluster framework $[H_4W_{22}O_{74}]$ can unambiguously be assigned as being present. The broad spectrum is simply due to the presence of several overlapping species arising from the many different envelopes. All these species are ions with a charge of 3– containing different amounts of sodium ions and protons. On lowering the pH to 2.4, a related "∫"-shaped $[H_{10}W_{34}O_{116}]^{18-}$ cluster is isolated as $Na_{18}[H_{10}W_{34}O_{116}] \cdot 47H_2O$ (Figure 1.8). The cluster framework $[H_{10}W_{34}O_{116}]$ can unambiguously be assigned as being present. Similarly, the broad spectrum is simply due to the presence of several overlapping species with different extents of protonation and hydration, which give many different distribution envelopes. The observation of such complex isopolytungstate-based clusters under electrospray conditions was not expected because of the number of possible species and the fragile nature of such clusters, but at the same time this offers many new possibilities for the systematic screening of reactions to discover new cluster architectures.

Another example recently reported by our group is the identification in solution of Nb_xO_y reaction mixtures. More specifically, we conducted the hydrothermal experiment over 20 h, using $\{Nb_6\}$ as the precursor, and then treated the mother liquor with hexadecyltrimethylammonium bromide. This procedure was intended to produce a material that could be dissolved in acetonitrile for analysis by high-resolution ESI-MS. These experiments resulted in the observation of a series of envelopes that could be assigned to $\{Nb_6\}$, $\{Nb_{10}\}$, $\{Nb_{20}\}$, and $\{Nb_{27}\}$. Although the $\{Nb_6\}$ was still present as the main component, it was possible to identify unambiguously a range of species that could be assigned as the $\{Nb_{27}\}$-based

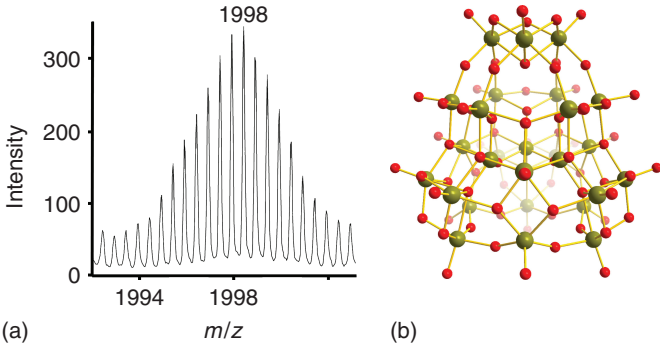

Figure 1.9 (a) Ball-and-stick representation of the structure of $\{Nb_{27}\}$. Color scheme: Nb, dark yellow and O, red spheres. (b) Distribution envelope of the $\{Nb_{27}\}$ species identified unambiguously in the reaction mixture.

anions (Figure 1.9) [18a]. This finding clearly indicates that a gradual molecular growth takes place via the lower nuclearity species toward the final formation of the $\{Nb_{27}\}$ cluster, which is the biggest isopolyoxoniobate species identified by ESI-MS in solution so far.

1.3.4
Solution Identification and Isolation of Mixed-Metal/Valence POMs with CSI-MS

The above examples show that ESI-MS studies have been extremely helpful in the identification of the composition, the extent of protonation, and the existence of other relatively stable species in the solution. However, these studies can be limited when we have to deal with labile clusters with complex compositions, or those that adopt large and unstable motifs. While a significant result was not obtained from the conventional ESI-MS of the subsequently discussed fragile species presumably due to the high desolvation plate temperature (180 °C), multiply charged high-nuclearity molecular ions were clearly observed without decomposition under CSI-MS conditions. Furthermore, given the extent of ionization and instability issues of such structures at high temperatures, it is often difficult to establish the presence of some cluster architectures using ESI-MS. In contrast, the low temperatures accessible (up to −100 °C) for use with a cryospray source minimize uncontrolled fragmentation and allow efficient transfer of very high nuclearity, yet labile, ionic species into the detector with minimal interference from the ionization and desolvation processes. Moreover, low temperatures allow the detection and entrapment of short-lived intermediate species that take part in a reaction mechanism, which is impossible to observe or to prove their existence using conventional methods. By employing this approach, it is then possible to transfer many of the labile and/or unstable species present in solution into the mass spectrometer and allow some correlation between the essentially gas-phase measurements and those

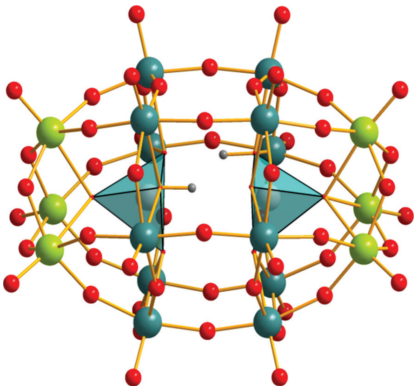

Figure 1.10 Representation of the isostructural anionic framework found in the structures of compounds with the general formula $[H_2V^{IV}M_{17}O_{54}(V^{V}O_4)_2]^{6-}$ (M = W or Mo). The $\{M_{17}V_1\}$ framework is shown in ball and stick and the V templates are shown by the polyhedra. Even though the "framework" V^{IV} ion cannot be formally located, theoretical calculations showed a preference for the two cap positions rather than the belt positions. Color scheme: Mo/W, dark green (belt), light green (cap); O, red; and V, dark green polyhedra [17a].

in the solution and solid state [26]. At this point, CSI-MS studies can offer the necessary environment for labile/unstable species to survive and collect important information which will help us understand the self-assembly mechanisms in supramolecular chemistry.

1.3.5
Mixed-Metal/Valence Hetero-POMs $V_2 \subset \{M_{17}V_1\}$

Over the last two years, we reported our first attempts to detect and study labile POM systems using CSI-MS. CSI-MS studies proved to be a tool of vital importance in first identifying these species using the correct combination of experimental parameters to minimize fragmentation allowing observation of new cluster architectures in solution, and then providing some indication of how the synthetic procedure can be optimized to yield the new architecture [17]. In this work, we aimed to replace the hetero-anion templates in the classical Dawson-like clusters, for example, $[W^{VI}{}_{18}O_{54}(PO_4)_2]^{6-}$, with transition metals; by scanning the reaction mixtures before crystallization, we were able to locate the reaction systems that produced the $V_2 \subset \{M_{17}V_1\}$ species, as shown in Figure 1.10.

The discovery studies were performed by precipitating solids from a range of candidate reaction systems under aqueous conditions. The precipitates were then transferred into the organic phase by ion exchange with TBA and "screened" using CSI-MS. These studies showed that this family of clusters was present in solution prior to their structural analysis. The studies also showed that the TBA salts of the $\{M_{17}V_3\}$(M = W, Mo) clusters were stable in solution (Figure 1.11). A range of charge (−1 to−3) and protonation (0–2) states were observed. Also, the direct

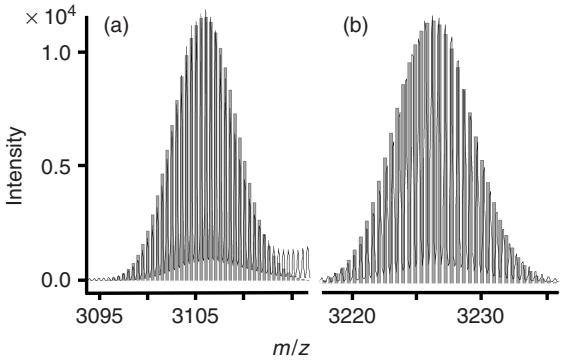

Figure 1.11 Positive ion mass spectrum showing the $\{(TBA)_{10-n}[H_nV_3W_{17}O_{62}]\}^{2+}$ in acetonitrile solution. (a) where $n = 2$ at m/z about 3106. (b) where $n = 1$ m/z about 3227. The black line shows the actual spectrum and the grey bar graph is the predicted envelop.

observation of $\{(TBA)_8[H_2V^V{}_2V^{IV}W_{17}O_{62}]\}^{2+}$ allowed us to confirm that the clusters observed in the solid state all have six cations associated and are di-protonated. This observation is useful since this gives unambiguous proof that the Dawson capsules are present in solution, establishes the existence of exactly one vanadium metal center on the shell of the Dawson framework (which is almost impossible to distinguish crystallographically), and also confirms the extent of protonation of the cluster, which is extremely difficult to determine directly.

Another challenging case is the mixed-metal/valence sulfite POM systems. The discovery of such species in solution, characterization, and final optimization of the synthetic conditions proved to be an intriguing task. In this investigation, CSI-MS proved to be an important technique in our efforts to discover new Dawson-like capsules in solution, allowing the compound to be identified prior to structural analysis [17b]. CSI-MS studies of the tetrapropylammonium (TPA) salts of the cluster (Figure 1.13) dissolved in acetonitrile confirmed that the sulfite capsule retained its integrity in solution, and the peaks seen were assigned to $\{(TPA)_4[H_{1-n}V^V{}_{5+n}V^{IV}{}_{2-n}Mo_{11}O_{52}(SO_3)]\}^{2-}$ where $n = 1$ (with only one vanadium ion in oxidation state IV), giving an envelope centered at m/z about 1534.5, and where $n = 0$ (with two vanadium ions in oxidation state IV, requiring one proton), giving an envelope centered at m/z about 1535.0 (Figure 1.12).

In the majority of the cases, effort to increase the cluster's solubility in organic solvents via cation exchange process is desirable, since the use of aqueous solutions can cause ion-transfer problems resulting in very low-intensity signals, which can be difficult to analyze in detail. Furthermore, aqueous reaction mixtures often results in the observation of a plethora of species resulting from the multitude of possibilities arising from the clusters transferring into the MS detector with sodium and potassium cations with multiple water ligands.

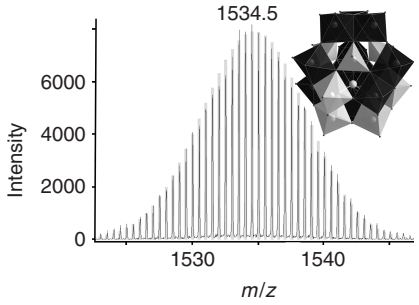

Figure 1.12 Negative ion mass spectrum in acetonitrile solution of $\{(Pr_4N)_4[H_{1-n}V^{V}_{5+n}V^{IV}_{2-n}Mo_{11}O_{52}(SO_3)]\}^{2-}$. Two envelopes can be seen where $n = 1$ (with only one vanadium ion in oxidation state IV) giving an envelope centered at *m/z* about 1534.5, and where $n = 0$ (with two vanadium ions in oxidation state IV, requiring one proton) giving an envelope centered at *m/z* about 1535.0. Black line: experimental data, light grey bars: simulation of isotope pattern. Inset: polyhedral representation of the anion. Color scheme: Mo, dark grey polyhedra; V, light grey polyhedra; and S, light grey sphere.

In an effort to extend the work on mixed-metal POM-based sulfite capsules, we managed to adjust appropriately the experimental conditions, which led to a molecular evolution of the $\{Mo_{11}V_7\}$ Dawson-like capsule to a ''crowned'' version of it with the formula $[Mo^{VI}{}_{11}V^{V}{}_5V^{IV}{}_2O_{52}(\mu_9 - SO_3)(Mo^{VI}{}_6V^{V}O_{22})]^{10-}$ [17d]. Following a similar approach and using as starting material the $\{Mo_{11}V_7\}$ capsule, it was possible to identify the new species in solution by CSI-MS. By fine adjustment of the solution's concentration, we managed to optimize the synthetic procedure and characterize the material in solid state by XRD analysis (Figure 1.13).

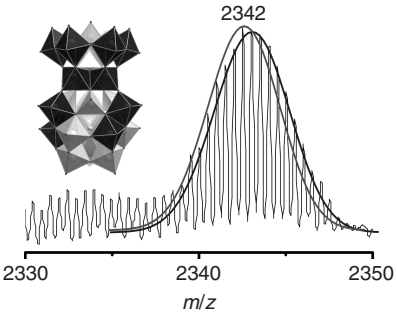

Figure 1.13 Negative ion mass spectrum in acetonitrile solution of $\{(Pr_4N)_7H_n[Mo^{VI}{}_{11}V^{V}{}_{5-n}V^{IV}{}_{2+n}O_{52}(\mu_9 - SO_3)(Mo^{VI}{}_6V^{V}O_{22})](NH_4)_2(CH_3CN)\}^{2-}$. Two envelopes can be seen where $n = 0$ (with only two vanadium ions in oxidation state IV) giving an envelope centered at *m/z* about 2342.1, and where $n = 1$ (with three vanadium ions in oxidation state IV, requiring three protons) giving an envelope centered at *m/z* about 2342.6. Black line: experimental data, Black/grey lines: profile lines of the simulated isotope patterns. Inset: polyhedral presentation of $\{Mo_{17}V_8\}$ capsule. Color scheme: Mo, dark grey polyhedra; V, light grey polyhedra; and S, light grey sphere.

The above examples demonstrate that the application of CSI-MS to investigate and discover labile or unstable cluster species in solution was used to help discover and then optimize the synthetic approach to isolate the clusters, and this proved to be of major significance. That became obvious when we carried out the same studies in the ESI mode on the same series of solutions, where in most of the cases the results were inconclusive owing to excessive fragmentation and led to a mixture of many different kinds of species revealing different compositions, oxidation states, and possible structures, making the assigning process impossible. The fine adjustment of the experimental conditions (concentrations, pH, and temperature) allows the direct observation of the species present in the reaction system using the CSI-MS technique: an approach that we have found useful to observe reactive building blocks and high-nuclearity clusters. In this context, we are utilizing CSI-MS to identify new POM clusters with novel templates and architectures that would not be easily isolated without prior detailed knowledge of the clusters present in the reaction solutions.

1.3.6
Periodate-Containing POMs

In an extension of this technique to look at reactive clusters, we utilized CSI-MS studies to identify and unambiguously reveal the composition of a new cluster species in solution and investigate the relationship between the solution and solid states. In this work, we explored the insertion of new high-oxidation-state guests into the ''Dawson capsule'' to allow modulation of the cluster's physical properties, for example, redox and catalytic properties, and acidity. The encapsulation of such templates should significantly affect the acidic, catalytic, and redox properties of the resulting cluster systems. In this work, we examined the tungsten Dawson capsule, $K_6[H_3W_{18}O_{56}(IO_6)] \cdot 9H_2O$, which we have both synthesized and characterized in the solid state [38]. To rule out the possibility that the aforementioned compound could be assigned as $[H_4W_{19}O_{62}]^{6-}$ (i.e., I substituted for W or other hetero-ions of comparable ionic radius), we utilized high-resolution CSI and ESI-MS to identify the exact elemental composition of the cluster anion. To simplify the MS experiments, the potassium salt of the aforementioned compound was ion-exchanged with TPA^+ cations, yielding $(TPA)_6[H_3W_{18}O_{56}(IO_6)]$. Figure 1.14 shows the mass spectrum of $(TPA)_6[H_3W_{18}O_{56}(IO_6)]$ in acetonitrile in which all major peaks are related to the $\{W_{18}I\}$ capsule. In contrast, the TPA^+ salt of $[H_4W_{19}O_{62}]^{6-}$ [39] capsule in acetonitrile gives a different mass spectrum in the same m/z region. Therefore, CSI mass spectral studies, in combination with elemental analysis and crystallography, have given us unambiguous proof of the existence and integrity of $\{W_{18}I\}$ species.

1.3.7
Probing the Formation of POM-Based Nano-Structures

The extension of MS studies to supramolecular architectures poses several important questions regarding the nature of the assemblies present in solution

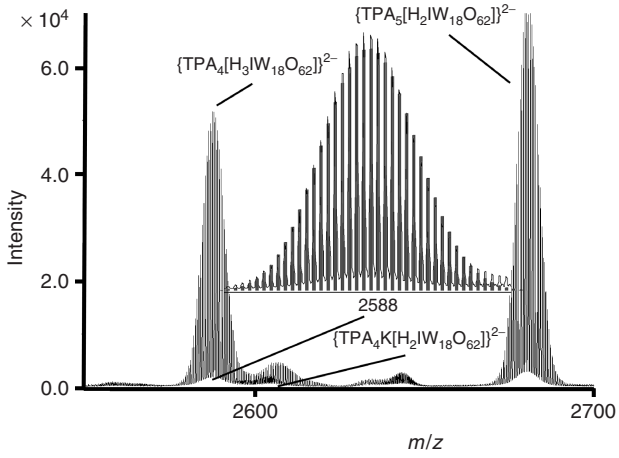

Figure 1.14 Negative-mode mass spectra of $(TPA)_6[H_3IW_{18}O_{62}]$ in acetonitrile. An expansion of the peak at $m/z = 2588$ is shown along with the calculated isotopic pattern (light grey bars).

versus those transmitted and observed in ESI-MS experiments. However, we have also made progress here as shown by the synthesis and characterization of a nano-structured POM-based assembly in the solid state [40]. By grafting of a H-bonding donor ''cap'' onto a POM cluster, we could control the supramolecular self-assembly of cluster species in solution, as well as in the solid state, leading to the formation of macromolecular H-bonded nano-assemblies of hybrid POM clusters. Most importantly, it was observed that the formation of these supramolecular architectures could be externally controlled by simply changing the grafted H-bonding organic cap (Figure 1.15).

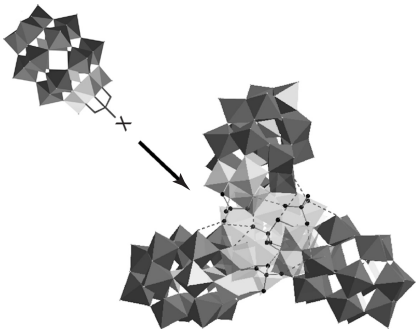

Figure 1.15 Hydrogen-bonded distorted tetrahedral nano-assembly of $[H_2NC(CH_2O)_3P_2V_3W_{15}O_{59}]^{6-}$ cluster. One lobe of the tetrahedron – pointing toward the observer – is made transparent for easy visualization of the H-bonding interactions. Color scheme: O, dark grey spheres; W, dark grey polyhedra; V, light grey polyhedra; and PO_4, grey polyhedral within the capsules, where X: $-NH_2$, $-NO_2$, and $-CH_3$.

In this case, CSI-MS studies did not only help us to identify and establish the integrity of the cluster but also to observe the formation of hydrogen-bonded nanostructures in the solution as well as to reveal information about the mechanism of this self-assembly process. By using cryospray experiments at −40 °C, we were able to examine the self-assembly processes in solution in great detail. For instance, CSI-MS studies of $(TBA)_4H_2[H_2NC(CH_2O)_3P_2V_3W_{15}O_{59}]$ in dilute acetonitrile solutions revealed that the tris(hydroxymethyl)-aminomethane-grafted POM cluster exists in solution phase as monomers, dimers, and trimers, and also the tetramer could be clearly observed. The observed mass and charge corresponding to each of these peaks clearly matched with the assigned formulae as well as the simulated spectra. The role of the H-bonding ability of the organic cap of the cluster anions in forming the multiple aggregation of cluster species in solution and gas phase was examined by comparing the CSI-MS of cluster species $[H_2NC(CH_2O)_3P_2V_3W_{15}O_{59}]^{6-}$ (**1**), $[O_2NC(CH_2O)_3P_2V_3W_{15}O_{59}]^{6-}$ (**2**), and $[H_3CC(CH_2O)_3P_2V_3W_{15}O_{59}]^{6-}$ (**3**) under identical experimental conditions. It was observed that the $-NO_2$-tipped cluster (**2**) also forms multiple aggregates in solution and gas phases, quite similar to cluster (**1**). Interestingly, it was found that the $-NO_2$ capped cluster is more efficient in forming such multiple aggregates in solution since assemblies of five (pentamer) and even six (hexamer) alkoxy POM clusters are observed. The weakly hydrogen-bonding $-CH_3$-tipped cluster forms mainly monomeric species in solution, and no higher aggregates are observed (Figure 1.16).

The aforementioned CSI-MS studies presented an approach to observe the formation of nano-assemblies of POM clusters in solution and in the gas phase and have given us important missing information on the ''mechanism'' that governs this assembly process. The outcome of this study allowed us to modify accordingly the extent of the H-bond network and consequently to control the interaction between nano-sized molecules. Furthermore, the observation of the gigantic hydrogen-bonded tetrahedral nano-assembly of the alkoxy cluster anions of $[H_2NC(CH_2O)_3P_2V_3W_{15}O_{59}]^{6-}$ along with 19 TBA counterions in solution phase by CSI-MS analysis underlines the potential of this technique to investigate the role of weak interactions such as hydrogen bonding in understanding the self-organization processes involved in the synthesis of novel POM-based functional nanomaterials.

1.3.8
Mechanistic Insights into POM Self-Assembly Using ESI- and CSI-MS

Given the power of CSI-MS to look in detail at labile POM solutions, we envisaged utilizing this technique to shed light upon the mechanism of self-organization of individual POM molecules from its reagents in solution. The study of the self-assembly processes of POMs has previously been pursued by the use of ligands with well-defined binding sites. This allows easier elucidation of the assembly processes, as the POM units effectively behave like multidentate organic ligands and bind readily to secondary transition metals [41]. It was for these reasons that the use of silver(I) cations as linking groups between POM units has been investigated by our group. It was found that, in the reaction of $[TBA_2(Mo_6O_{19})]$ with silver(I)

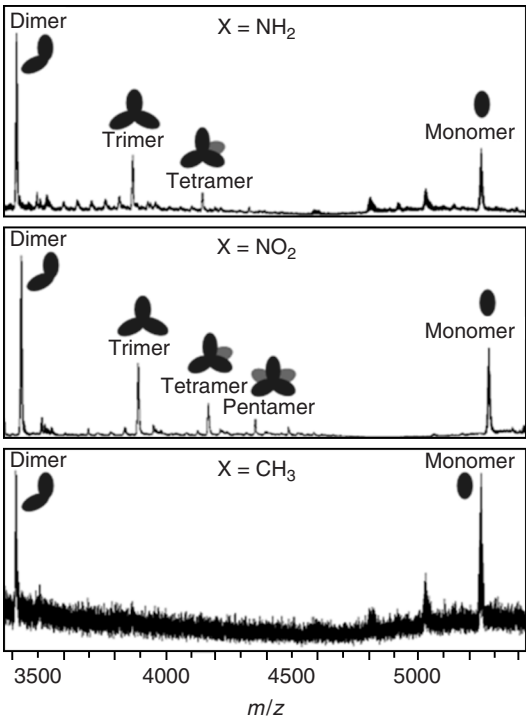

Figure 1.16 Comparison of the CSI-MS spectra and supramolecular assemblies of clusters **1**($-NH_2$), **2**($-NO_2$), and **3**($-CH_3$) as a function of different substituent (X) on the organic cap. Spectra are on the same *m/z* scale.

fluoride in a mixed acetonitrile–methanol solution, a unique one-dimensional chain structure of the composition $(TBA_{2n}[Ag_2Mo_8O_{26}]_n)$ is produced. Furthermore, many other architectures, involving specifically the aggregation of $\{Ag(Mo_8)Ag\}$ synthons, have been produced [42]. In this work, the in-solution interconversion of Lindqvist into β-octamolybdate anions and subsequent self-assembly into the silver-linked POM structure $[(n-(C_4H_9)_4N)_{2n}(Ag_2Mo_8O_{26})_n]$ was investigated using CSI-MS and electronic absorbance spectroscopy [43], allowing the direct monitoring of real-time rearrangements in the reaction mixture. Only mono-anionic and di-anionic series were observed in these results, from approximately *m/z* 285 to as high as approximately *m/z* 3800, indicating the efficient transfer of very high nuclearity, yet labile, ionic species into the detector with minimal interference from the ionization and desolvation processes. Of these identified anion series (see Figure 1.17), only $[HMo_mO_{3m+1}]^-$ series had been observed in previous ESI-MS studies on polyoxomolybdate systems [21], which underpins the advance in understanding that can be made with CSI-MS studies for detecting molecular building blocks. The $[H_7Mo_mO_{3m+3}]^-$ series is of special interest with regard to this POM reaction system. This is because the role of the AgI moiety in the assembly of the

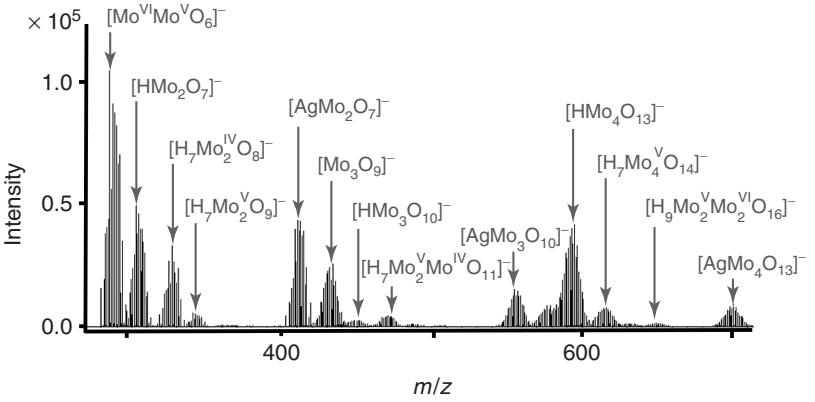

Figure 1.17 CSI-MS data collected for the reaction solution. The six mono-anionic series identified within these results are highlighted. The steps toward the assembly of the {Ag(Mo$_8$)Ag} synthon units can be observed by examination of anion series (vi), which highlights the role of the Ag^+ in the rearrangement process of these clusters. Of particular note from this series are the peaks at *m/z* 410.7 and 700.5, which are attributed to the species $[AgMo_2O_7]^-$ and $[AgMo_4O_{13}]^-$, respectively.

stable silver-linked octamolybdate species has been established by mass spectral methods for the first time and is shown to be crucial for the formation of the larger cluster fragments.

Detection of the $[AgMo_2O_7]^-$ fragment (peak at *m/z* 410) of the (Ag{Mo$_8$}Ag) synthon from the reaction solution supports the theory of rearrangement of the Lindqvist anion into $[AgMo_2O_7]^{-n}$, which is the smallest stable unit of the silver-linked POM chain. Indeed, the stable nature of this fragment of the (Ag{Mo$_8$}Ag) synthon unit allowed the isolation in the solid state of $Ag_2Mo_2O_7$ clusters linked into 1D chains, which has been reported by Gatehouse and Leverett [44]. Detection of the $[AgMo_4O_{13}]^-$ species (peak at *m/z* 700.5), being half of the (Ag{Mo$_8$}Ag) synthon unit, represents the next stepping stone in the final rearrangement to the stable silver-linked octamolybdate species.

In the higher mass range of the CSI-MS analyses carried out, the structure-directing effect of the organic cations has been illustrated for the first time. Detection of the species $[(AgMo_8O_{26})TBA_2]^-$ (peak at *m/z* 1776.6), $[(Ag_2Mo_8O_{26})(Mo_4O_{13})TBA_3]^-$ (peak at *m/z* 2718.3), and $[(Ag_2Mo_8O_{26})(Mo_8O_{26})TBA_5]^-$ (peak at *m/z* 3796.5), each with an increasing organic cation contribution, shows the increasing metal nuclearity of the chain of polymer compound concomitant with the associated increase in organic cations present (Figure 1.18). This observation can be interpreted as the start of the self-assembly aggregation process where ''monomeric'' units assemble into larger fragments, which eventually leads to the formation of crystals of the compound $(TBA_{2n}[Ag_2Mo_8O_{26}]_n)$. Kinetics of the rearrangement process of Lindqvist anions into (Ag{Mo$_8$}Ag) synthons in the reaction solution was studied using electronic absorbance measurements. The relationship between decreasing Lindqvist anion concentration and concomitant

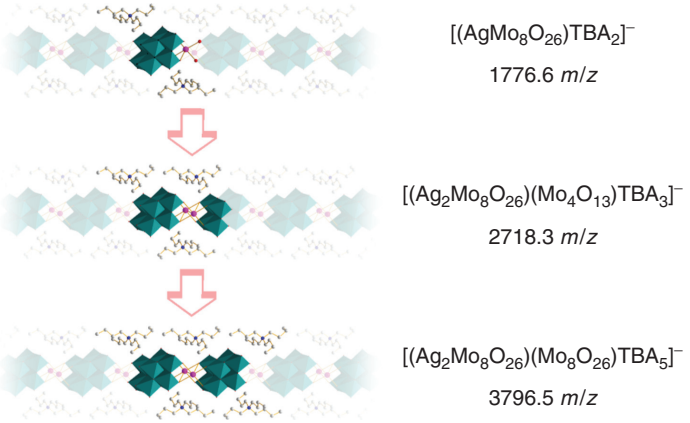

Figure 1.18 Structural representation of the higher mass fragments (highlighted) identified within the CSI-MS analyses of a reaction solution. This diagram illustrates the increasing metal nuclearity of the chain concomitant with the associated increase in organic cations present. Color scheme: Mo, green polyhedra; Ag, pink; O, red; C, gray; and N, blue.

increase in {Mo_8} anion concentration was further supported by monitoring the reaction solution over time using CSI-MS experiments.

In summary, the use of CSI-MS in this way to monitor in real-time, in-solution rearrangements in a POM reactant solution is, to our knowledge, unprecedented. This approach can be extended to investigate the bottom-up, in-solution processes governing the formation of other POM systems, enhancing our understanding and giving us the potential to control the building-block principles involved.

In an effort to monitor the reaction mixture and investigate the formation mechanism of a more complicated POM-based chemical system, we utilized the ESI-MS technique to investigate, in real time, the formation of a complex and organic–inorganic POM hybrid system. The reaction system chosen for investigation in this case was found by Hasenknopf *et al.* [45] and involves the rearrangement of $[\alpha\text{-}Mo_8O_{26}]^{4-}$, coordination of Mn^{III}, and coordination of two tris(hydroxylmethyl)aminomethane (TRIS) molecules, to form the symmetrical Mn-Anderson cluster $TBA_3[MnMo_6O_{18}((OCH_2)_3CNH_2)_2]$. This piece of work [46] is very important since the organic–inorganic POM hybrids can be used as synthons in the design of nanoscale hybrid POM architectures, thereby increasing our knowledge of the aggregation processes that form such building blocks and making the field of nanoscale functional materials more accessible for further exploration.

The speciation and fragment rearrangements were investigated, and the first spectrum was dominated by peaks that could be assigned to isopolyoxomolybdate fragments of the rearranging $[\alpha\text{-}Mo_8O_{26}]^{4-}$ anion (Figure 1.19). The dominance of these isopolyoxomolybdate fragments indicates that the $[\alpha\text{-}Mo_8O_{26}]^{4-}$ anion rearranges into these smaller fragment ions prior to further coordination with

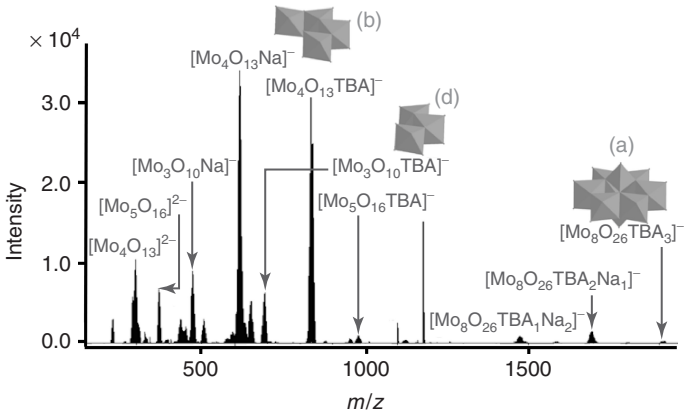

Figure 1.19 ESI-MS spectra collected of the reaction solution of $[\alpha\text{-}Mo_8O_{26}]^{4-}$, recorded after stirring at room temperature for 13 min. The spectrum is dominated by isopolyoxomolybdate fragment peaks. Of particular note are the two major peaks in this spectrum, at *m/z* 614.6 (the base peak) and 833.8, which are attributed to the species $[Mo_4O_{13}Na]^-$ and $[Mo_4O_{13}TBA]^-$ respectively, that is, half of the parent $(Mo_8O_{26})^{4-}$ cluster anion. Some of the intermediate prominent fragment ions are also shown here and are labeled similarly. Color scheme: Mo, dark grey polyhedra; and O, dark grey spheres. Structural representations: (a) $[\alpha\text{-}Mo_8O_{26}]^{4-}$, (b) $[Mo_4O_{13}TBA]^-$, and (d) $[Mo_3O_{10}TBA]^-$.

the Mn cations and TRIS groups. Indeed, the first indications of this further coordination are illustrated by the presence of very low-intensity peaks containing TRIS groups and manganese cations, for example, $[Mo_2O_5((OCH_2)_3CNH_2)]^-$ (*m/z* 387.8) and $[Mn^{III}Mo_3O_8((OCH_2)_3CNH_2)_2]^-$ (*m/z* 706.7).

The complexity and ion series observed in this spectrum remain observable through to the final spectrum recorded after refluxing for approximately 30 h (see Figure 1.20). It is interesting to note at this point the presence of Mn^{II} ions, particularly in the smaller *m/z* fragment ions, and mixed oxidation state species where molybdenum is found to exist in oxidation states IV–VI. Observation of molybdenum and manganese centers in reduced oxidation states is not entirely unexpected because of the high voltages utilized in the mass spectrometer during the ion-transfer process [47]. Also, a singly reduced molybdate species $[Mo^VO_3]^-$, and the corresponding singly reduced tungstate species $[W^VO_6]^-$, has been observed in previous studies, along with mixed oxidation state fragments of polyoxomolybdate ions [47].

In this work, it is rather important to note that further information about the rearrangement processes taking place in solution from $[\alpha\text{-}Mo_8O_{26}]^{4-}$ through to the formation of the product cluster anion $[MnMo_6O_{18}((OCH_2)_3CNH_2)_2]^{3-}$ can be reliably extracted from the ESI-MS by monitoring the reaction as a function of time. These observations, when considered as a whole, are crucial in the effort to increase our understanding of the rearrangement processes taking place in the reaction solution. First, the exponential decrease in peak intensity of the $[Mo_8O_{26}TBA_3]^-$ and the $[Mo_4O_{13}TBA]^-$ ions could

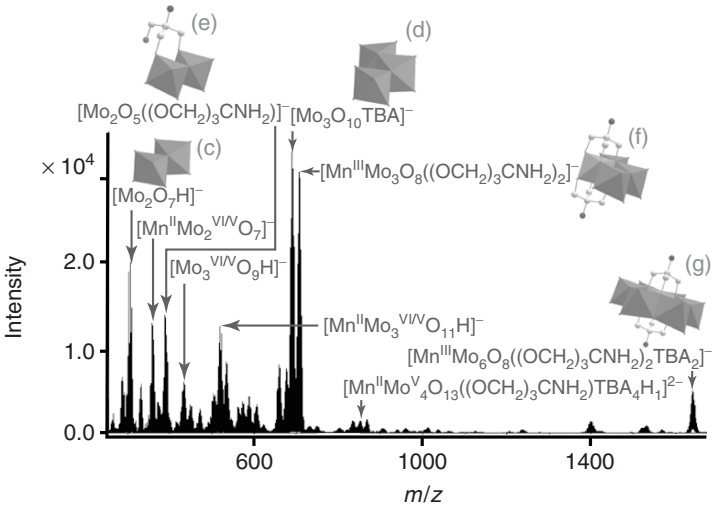

Figure 1.20 ESI-MS spectra collected of the reaction solution of $[\alpha\text{-}Mo_8O_{26}]^{4-}$, recorded after refluxing at 80 °C for approximately 30 h. Some of the intermediate prominent fragment ions are also shown here and are labeled similarly. Color scheme: Mo, dark grey polyhedra; Mn, grey polyhedra; O, grey spheres; N, dark grey spheres; and C, light grey. H atoms are omitted for clarity. Structural representation: (c) $[Mo_2O_7H]^-$, (d) $[Mo_3O_{10}TBA]^-$, (e) $[Mo_2O_5((OCH_2)_3CNH_2)]^-$, (f) $[Mn^{III}Mo_3O_8((OCH_2)_3CNH_2)_2]^-$, and (g) $[MnMo_6O_{18}((OCH_2)_3CNH_2)_2]^{3-}$.

suggest an initial rapid decomposition and rearrangement of the $[\alpha\text{-}Mo_8O_{26}]^{4-}$ via the formation of the $[Mo_4O_{13}]^{2-}$ cluster species, that is, $[Mo_4O_{13}Na_1]^-$ (*m/z* 614.6, base peak) and $[Mo_4O_{13}TBA]^-$ (*m/z* 833.8), which are half fragments of the $\{\alpha\text{-}Mo_8\}$ clusters and the most prominent peaks in the first spectrum recorded (see Figure 1.20), into the smaller, stable dinuclear, that is, $[Mo_2O_7H]^-$, and trinuclear, that is, $[Mo_3O_{10}TBA]^-$, isopolyoxomolybdate fragments. The concomitant increase in peak intensity of these small isopolyoxomolybdate ions over the time of reaction supports this proposal. Then the identification of similar dinuclear and trinuclear molybdate fragments possessing further coordination with TRIS and manganese ions, that is, $[Mo_2O_5((OCH_2)_3CNH_2)]^-$ and $[Mn^{III}Mo_3O_8((OCH_2)_3CNH_2)_2]^-$, and whose concentrations also increase over the time of reaction, suggests subsequent coordination of these building blocks with TRIS, manganese ions, and further molybdate anionic units, thereby building up the final Mn-Anderson-TRIS product ion.

The aforementioned cases demonstrate that the utilization of real-time mass spectrometry opens the door to investigations of even more complex chemical systems. Generally, the application of this approach to a wide range of nanomolecular systems will improve our understanding of the self-assembly processes and allow us to design efficient synthetic procedures which would lead to the formation of complex functional architectures.

1.4
Species Identification and Probing Structural Transformations in Multi-Metallic Systems

The diversity and effectiveness of CSI-MS studies has also been proven in the case of multi-metallic coordination systems. Careful scanning of $\{Co_{(12-x)}Ni_x\}$–tach (where tach is *cis,trans*-1,3,5-triaminocyclohexane) reaction mixtures of different concentration ratios allowed us to isolate the correct reaction conditions, which led to the identification, characterization, and finally the formation of pure desirable products [48]. The existence of a combinatorial library of Co–Ni species makes the system extremely difficult to characterize, yet allows us to design multinuclear bimetallic magnetic materials. Close examination of the ESI-MS data of the identified compounds clearly shows envelopes corresponding to the $\{Ni_{12}\}$ and $\{Co_{12}\}$ intact cluster species, which can each be assigned as $[Ni_{12}(CH_3O)_{12}(CH_3CO_2)_9(CO_3)(tach)_6]^+$ and $[Co_{12}(OH)_{12}(CH_3CO_2)_{10}(CO_3)(H_2O)_6(tach)_6(H)]^+$ (Figure 1.21). Furthermore, the $\{Co_6Ni_6\}$ species gives a CSI-MS envelope which matches that expected for a discrete mixed species (containing $(OH)_6$ and $(CH_3O)_6$ groups), rather than the supposition of many possible outcomes. Moreover, we found that isostructural mixed Ni–Co clusters could be accessed by controlling the pH–metal ion ratio of the reaction solution after studying the system by CSI-MS, and these mixed systems can be observed using MS and isolated in the pH range of 3.5–10.5 (Figure 1.22) as a function of pH and concentration ratios.

Using the same conditions and solution identification technique, we managed to isolate the $\{Co_{13}\}$ species (Figure 1.23, left), which represents the same structural motif with the aforementioned $\{M_{12}\}$ compounds and consists of three Co-cubanes that are bridged together through a $[CoO_3(OAc)]^{5-}$ unit. Utilizing CSI-MS studies,

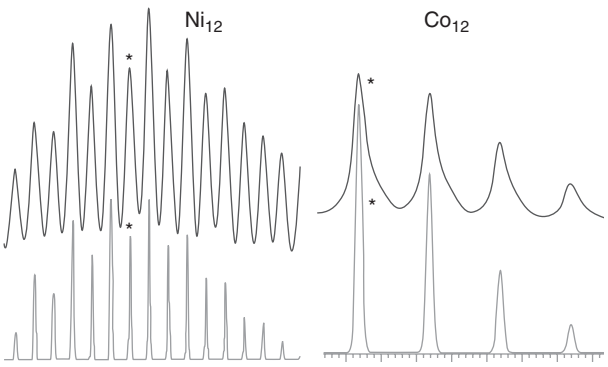

Figure 1.21 Cryospray mass spectrum for the $\{M_{12}\}$ clusters at −40 °C. Experimental (top) and simulated data (below). (b) $[Co_{12}(OH)_{12}(CH_3CO_2)_{10}(CO_3)(H_2O)_6(tach)_6H]^+$;* = m/z 2445. (a) $Ni_{12}(CH_3O)_{12}(CH_3CO_2)_9(CO_3)(tach)_6]^+$; * = m/z 2442 (simulated and experimental within 1 Da).

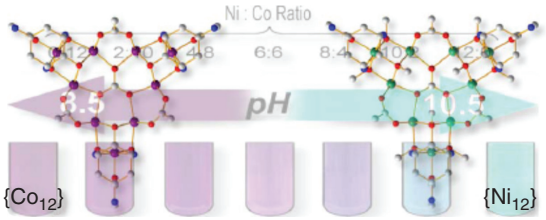

Figure 1.22 Structures of the $\{Co_{12}\}$ and $\{Ni_{12}\}$ complexes and a schematic showing the colors of mixed $\{Ni_{12-n}Co_n\}$ ($n = 1, 2, \ldots, 11$) intermediates. Color scheme: Ni, green; Co, purple; C, gray; N, blue; and O, red.

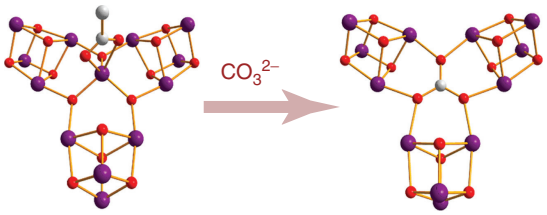

Figure 1.23 Comparison of cores of $\{Co_{13}\}$ (left) and $\{Co_{12}\}$ (right), capping *trans*-tach ligands omitted for clarity.

we observed the real-time structural transformation in solution of $\{Co_{13}\}$ to $\{Co_{12}\}$ daughter products by exchanging the central templating core $[CoO_3(OAc)]^{5-}$ for the carbonate anion (Figure 1.23) [48b]. The aforementioned observation also demonstrates that the $\{Co_{12}\}$ cluster core in solution originates from the $\{Co_{13}\}$ cluster core that forms in the absence of "external" ligand templates, giving us important hidden information about what takes place during the self-assembly process. The ability to induce systematic transformations to a given molecular framework or supramolecular architecture, that is, to fine-tune electronic or magnetic properties, is crucial in the design of functional molecule-based materials.

In another piece of work [49], the use of CSI-MS studies has allowed the identification of a multi-metallic Cr-based species in solution formed by reactive $\{Cr_6\}$ species, where the $\{Cr_6\}$ forms a larger complex via sodium fluoride interactions to give $[(NH_2Et_2)\{CrNa_{14}F_6(H_2O)_{10}\}\{Cr_6F_{11}(O_2CBu)_{10}\}_4]$. Although ESI-MS measurements did not allow the observation of the intact cluster, CSI-MS experiments on a $\{Cr_{25}\}$ (Figure 1.24) compound in THF:CH_3CN (70 : 30) at −40 °C showed that the supramolecular assembly is present as a di-cation. The parent cluster ion can be found in two overlapping envelopes centered at an m/z of about 3410.2. Two species can be identified that are related to the parent cluster. Both species are doubly charged and the observed pattern corresponds to (i) $C_{204}H_{390}NCr_{25}F_{48}Na_{14}O_{89}$ and (ii) $C_{204}H_{388}NCr_{25}F_{50}Na_{14}O_{87}$, respectively. The most unusual aspect of the aforementioned material is that the $\{Cr_6\}$ "horseshoe" acts as a poly-nucleating fluoride donor and that the resulting supramolecular assembly has significant

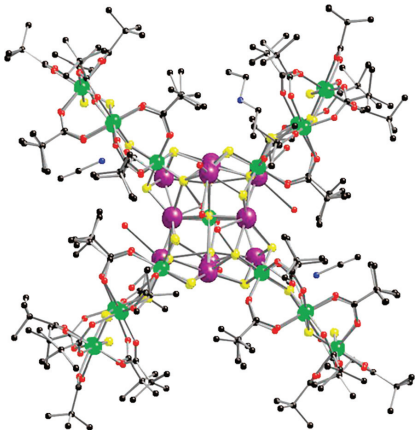

Figure 1.24 Crystal structure of $[(NH_2Et_2)\{CrNa_{14}F_6(H_2O)_{10}\}\{Cr_6F_{11}(O_2CBu)_{10}\}_4]$. Color scheme: Cr, green; O, red; F, yellow; N, blue; C, black; Na, purple; and H, not shown.

solution stability. CSI-MS is possibly the only tool currently available that can unambiguously demonstrate the structural integrity of this complex in solution.

CSI-MS can also be used to observe intact multi-metallic coordination complexes in solution, and this has been illustrated through the work investigating a novel pentanuclear palladium(II) complex [50]. For example, we have designed ligand L1 (see Figure 1.25) to interact with anionic species and to coordinate to metal ions. Interestingly, ligand L1 is transformed to L2 upon complexation. On reaction of compound L1 with palladium(II) acetate in dichloromethane (DCM), a pentanuclear Pd(II) complex is formed in which the Pd(II) mediates a ligand transformation of the aforementioned compound into a phenanthridone-based ligand (L2). The Pd(II) coordination compound has been characterized in the solid state via single-crystal X-ray crystallography and has been formulated as $[Pd_5(L_2)_2(OAc)_8](Br)_2$ (see Figure 1.26). CSI-MS investigations have also shown that the Pd_5L_2 core can be observed in the solution state by the identification of the $[Pd_5(C_{40}H_{34}N_{12}O)_2(CH_3CO_2)_5Cl_6]^-$ anion at −40 °C.

1.5 Future Challenges and Conclusions

In recent years, there has been an unprecedented rise in the number and size of interesting supramolecular clusters that have been structurally characterized by single-crystal X-ray crystallography. We showed that POMs and multi-metallic coordination compounds are ideal candidates for the development of a new type of supramolecular chemistry based upon the building-block ideas already established; using these ideas it should be possible to work toward designing nanomolecules

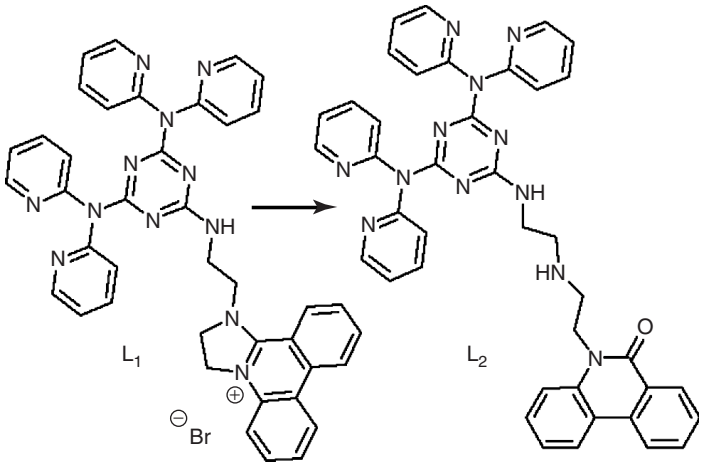

Figure 1.25 The transformation of compound L1 into L2 upon complexation with Pd(OAc)2 in DCM via a ring-opening process; this occurs in a 33% yield.

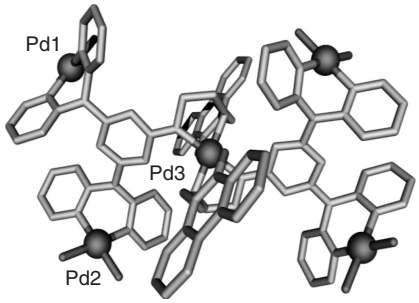

Figure 1.26 Ball-and-stick representation of $[Pd_5(L_2)_2(OAc)_8]^{2+}$. The solvent, anions of crystallization, and terminal acetate groups as well as the H atoms, are omitted for clarity. Color scheme: C, light grey sticks; N, grey sticks; O, dark grey sticks; and Pd, dark grey spheres. Pd_3 rests on an inversion center.

of increasing size and complexity. On the other hand, serendipity prevents us from designing the desirable functionality and manipulating the correct set of fundamental synthons under specific experimental conditions. In this chapter, we showed that, by utilizing the power of high-resolution ESI and CSI-MS to investigate very large labile frameworks, it is possible to overcome such drawbacks and promote further our understanding of the building-block principles and selection rules that govern the bottom-up self-assembly processes of inorganic complexes, supramolecular architectures, and cluster formation processes in solution. Although it is true that environmental conditions found in MS experiments differ

from ordinary synthetic procedures, we have found them to be increasingly able to correlate the data from the MS studies with solution data. This is especially relevant to intrinsically charged clusters/supramolecular architectures, but it is important to note that labile systems may be easily disturbed by MS experiment and only experiments with good controls can be used with confidence to directly probe the solution phase. Indeed, the validation of MS studies for direct probing of the species in solution is one important part of our ongoing research.

Furthermore, the extension of the use of ESI-MS and CSI-MS for identification of intermediate reactive species in many different reaction mechanisms could reveal an unprecedented level of information, allowing the monitoring and classification of the species that prevail under specific conditions and directing the bottom-up self-assembly of fundamental building blocks toward higher nuclearity species through a molecular evolution process. Moreover, we will soon introduce the new field of VT-MS by presenting the first results obtained from complex chemical systems, which will open the door for additional insight to the assembly processes by ''trapping'' the key reactive intermediates that are responsible for the final structural features and properties of the materials. The above extracted information will allow initially a correlation to be made between the isolated architecture and potentially the common intermediate species that exist in solution, of conceptually related chemical systems, which will give us the opportunity to create a library of these key intermediates for future reference and design. This is an important area for research, as our increasing knowledge of these formation mechanisms will allow us to design procedures and direct the synthesis of new POM-based and multinuclear coordination clusters that adopt specific architectures and exhibit desirable functionality.

Finally, the discoveries that have been discussed in this chapter clearly show that the first significant steps toward this goal have been accomplished, while the ultimate achievement for controlled and directed self-assembly of complex functional nanoscale chemical systems is brought one step closer by employing these techniques. We may even be able to directly use mass spectrometry to guide synthetic routes to isolate desired products, plan more effective synthetic procedures based on the extracted information by ESI and CSI-MS studies, and design novel procedures for synthesizing functional materials, thereby bridging the gap between self-assembly, serendipity, and designed synthesis.

References

1. Steed, J.W. and Atwood, J.L. (2000) *Supramolecular Chemistry*, John Wiley & Sons, Ltd, Chichester.
2. Sanchez, G., de Soler-Illia, G.J., Ribot, F., Lalot, T., Mayer, C.R., and Cabuil, V. (2001) *Chem. Mater.*, **13**, 3061.
3. Long, D.-L., Kögerler, P., Farrugia, L.J., and Cronin, L. (2003) *Angew. Chem. Int. Ed.*, **42**, 4180.
4. Long, D.-L., Tsunashima, R., and Cronin, L. (2010) *Angew. Chem. Int. Ed.*, **49**, 1736.
5. (a) Long, D.-L., Abbas, H., Kögerler, P., and Cronin, L. (2004) *J. Am. Chem. Soc.*, **126**, 13880; (b) Long, D.-L., Kögerler, P., and Cronin, L. (2004) *Angew. Chem. Int. Ed.*, **43**, 1817.

6. (a) Cronin, L., Kögerler, P., and Müller, A. (2000) *J. Solid State Chem.*, **152**, 57; (b) Hussain, F., Gable, R.W., Speldrich, M., Kögerler, P., and Boskovic, C. (2009) *Chem. Commun.*, 328; (c) Kögerler, P., Tsukerblat, B., and Müller, A. (2010) *Dalton Trans.*, **39**, 21; (d) Mal, S.S. and Kortz, U. (2005) *Angew. Chem. Int. Ed.*, **44**, 3777; (e) Bassil, B.S., Ibrahim, M., Sankar Mal, S., Suchopar, A., Ngo Biboum, R., Keita, B., Nadjo, L., Nellutla, S., van Tol, J., Dalal, N.S., and Kortz, U. (2010) *Inorg. Chem.*, **49**, 4949.
7. Winpenny, R.E.P. (2002) *J. Chem. Soc. Dalton Trans.*, 1.
8. (a) Pope, M.T. and Müller, A. (1991) *Angew. Chem. Int. Ed. Engl.*, **30**, 34; (b) Müller, A. and Roy S. (2004) in *The Chemistry of Nanomaterials: Synthesis, Properties and Applications* (eds C.N.R. Rao, A. Müller, and A.K. Cheetham), Wiley-VCH Verlag GmbH, Weinheim, pp. 452–475.
9. Hill, C.L. (1998) *Chem. Rev.*, **98**, 1.
10. Long, D.-L., Burkholder, E., and Cronin, L. (2007) *Chem. Soc. Rev.*, **36**, 105.
11. Hasenknopf, B. (2005) *Front. Biosci.*, **10**, 275.
12. (a) Long, D.-L., Abbas, H., Kögerler, P., and Cronin, L. (2004) *J. Am. Chem. Soc.*, **126**, 13880; (b) Miras, H.N., Yan, J., Long, D.-L., and Cronin, L. (2008) *Angew. Chem. Int. Ed.*, **47**, 8420; (c) Ritchie, C., Ferguson, A., Nojiri, H., Miras, H.N., Song, Y.-F., Long, D.-L., Burkholder, E., Murrie, M., Kögerler, P., Brechin, E.K., and Cronin, L. (2008) *Angew. Chem. Int. Ed.*, **47**, 5609.
13. (a) Miras, H.N., Cooper, G.J.T., Long, D.-L., Bögge, H., Müller, A., Streb, C., and Cronin, L. (2010) *Science*, **327**, 72; (b) Ritchie, C., Streb, C., Thiel, J., Mitchell, S.G., Miras, H.N., Long, D.-L., Boyd, T., Peacock, R.D., McGlone, T., and Cronin, L. (2008) *Angew. Chem. Int. Ed.*, **47**, 6881; (c) Long, D.-L., Streb, C., Song, Y.-F., Mitchell, S.G., and Cronin, L. (2008) *J. Am. Chem. Soc.*, **130**, 1830.
14. (a) Lehn, J.-M. (2007) *Chem. Soc. Rev.*, **36**, 151; (b) Lehn, J.-M. (2002) *Science*, **295**, 2400; (c) Lehn, J.-M. (1999) *Chem. Eur. J.*, **5**, 2455; (d) Lehn, J.-M. (1995) *Supramolecular Chemistry: Concepts and Perspectives*, Wiley-VCH Verlag GmbH, Weinheim; (e) Lehn, J.-M. (1978) *Acc. Chem. Res.*, **11**, 49.
15. (a) Pluth, M.D. and Raymond, K.N. (2007) *Chem. Soc. Rev.*, **36**, 161; (b) Saalfrank, M.R.W. and Demleitner, B. (1999) in *Perspectives in Supramolecular Chemistry*, vol. **5** (ed. J.-P. Sauvage), John Wiley & Sons, Ltd, Chichester, p. 1; (c) Holliday, B.J. and Mirkin, C.A. (2001) *Angew. Chem. Int. Ed.*, **40**, 2022; (d) Winpenny, R.E.P. (1999) in *Perspectives in Supramolecular Chemistry*, vol. **5** (ed. Sauvage, J.-P.), John Wiley & Sons, Ltd, Chichester, p. 193; (e) Cutland, A.D., Malkani, R.G., Kampf, J.W., and Pecoraro, V.L. (2000) *Angew. Chem. Int. Ed.*, **39**, 2689; (f) Miras, H.N., Chakraborty, I., and Raptis, R.G. (2010) *Chem. Commun.*, 2569; (g) Oshio, H., Hoshino, N., Ito, T., Nakano, M., Renz, F., and Gütlich, P. (2003) *Angew. Chem. Int. Ed.*, **42**, 223; (h) Watton, S.P., Fuhrmann, P., Pence, L.E., Caneschi, A., Cornia, A., Abbati, G.L., and Lippard, S.J. (1997) *Angew. Chem. Int. Ed. Engl.*, **36**, 2774.
16. (a) Seeber, G., Kögerler, P., Kariuki, B.M., and Cronin, L. (2004) *Chem. Commun.*, 1580; (b) Seeber, G., Kögerler, P., Kariuki, B.M., and Cronin, L. (2002) *Chem. Commun.*, 2912.
17. (a) Miras, H.N., Long, D.-L., Kögerler, P., and Cronin, L. (2008) *Dalton Trans.*, 214; (b) Miras, H.N., Nieves Corella Ochoa, M., Long, D.-L., and Cronin, L. (2010) *Chem. Commun.*, 8148; (c) Walanda, D.K., Burns, R.C., Lawrance, G.A., and Von Nagy-Felsobuki, E.I. (1999) *Inorg. Chem. Commun.*, **10**, 487; (d) Miras, H.N., Stone, D.J., McInnes, E.J.L., Raptis, R.G., Baran, P., Chilas, G.I., Sigalas, M.P., Kabanos, T.A., and Cronin, L. (2008) *Chem. Commun.*, 4703.
18. (a) Tsunashima, R., Long, D.-L., Miras, H.N., Gabb, D., Pradeep, C.P., and Cronin, L. (2010) *Angew. Chem. Int. Ed.*, **49**, 113; (b) Ohlin, C.A., Villa, E.M., Fettinger, J.C., and Casey, W.H. (2008) *Angew. Chem. Int. Ed.*, **47**, 5634.
19. Sahureka, F., Burns, R.C., and von Nagy-Felsobuki, E.I. (2003) *Inorg. Chim. Acta*, **351**, 69.

20. (a) Aubriet, F., Maunit, B., Courrier, B., and Muller, J.F. (1997) *Rapid Commun. Mass Spectrom.*, **11**, 1596; (b) Molek, K.S., Reed, Z.D., Ricks, A.M., and Duncan, M.A. (2007) *J. Phys. Chem. A*, **111**, 8080.
21. (a) Walanda, D.K., Burns, R.C., Lawrance, G.A., and Von Nagy-Felsobuki, E.I. (1999) *J. Chem. Soc. Dalton Trans.*, 311; (b) Alyea, E.C., Craig, D., Dance, I., Fisher, K., Willett, G., and Scudder, M. (2005) *CrystEngComm*, **7**, 491.
22. (a) Bonchio, M., Bortolini, O., Conte, V., and Sartorel, A. (2003) *Eur. J. Inorg. Chem.*, **4**, 699; (b) Walanda, D.K., Burns, R.C., Lawrance, G.A., and Von Nagy-Felsobuki, E.I. (2000) *J. Cluster Sci.*, **1**, 5.
23. Boglio, C., Lenoble, G., Duhayon, C., Hasenknopf, B., Thouvenot, R., Zhang, C., Howell, R.C., Burton-Pye, B.P., Francesconi, L.C., Lacote, E., Thorimbert, S., Malacria, M., Afonso, C., and Tabet, J.C. (2006) *Inorg. Chem.*, **3**, 1389.
24. (a) Mayer, C.R., Roch-Marchal, C., Lavanant, H., Thouvenot, R., Sellier, N., Blais, J.C., and Sécheresse, F. (2004) *Chem. Eur. J.*, **21**, 5517; (b) Dablemont, C., Proust, A., Thouvenot, R., Afonso, C., Fournier, F., and Tabet, J.C. (2004) *Inorg. Chem.*, **43**, 3514.
25. (a) Sahureka, F., Burns, R.C., and von Nagy-Felsobuki, E.I. (2002) *Inorg. Chem. Commun.*, **5**, 23; (b) Sahureka, F., Burns, R.C., and von Nagy-Felsobuki, E.I. (2001) *J. Am. Soc. Mass Spectrom.*, **10**, 1136.
26. Deery, M.J., Howarth, O.W., and Jennings, K.R.J. (1997) *Chem. Soc. Dalton Trans.*, 4783.
27. Colton, R. and Traeger, J.C. (1992) *Inorg. Chim. Acta*, **201**, 153.
28. Tuoi, J.L. and Muller, E. (1994) *Rapid Commun. Mass Spectrom.*, **9**, 692.
29. (a) Waters, T., O'Hair, R.A.J., and Wedd, A.G. (2003) *J. Am. Chem. Soc.*, **125**, 3384; (b) Waters, T., O'Hair, R.A.J., and Wedd, A.G. (2003) *Int. J. Mass Spectrom.*, **228**, 599; (c) Gun, J., Modestov, A., Lev, O., Saurenx, D., Vorotyntsev, M.A., and Poli, R. (2003) *Eur. J. Inorg. Chem.*, **3**, 482.
30. (a) Sakamoto, S., Fujita, M., Kim, K., and Yamaguchi, K. (2000) *Tetrahedron*, **56**, 955; (b) Saito, K., Sei, Y., Miki, S., and Yamaguchi, K. (2008) *Toxicon*, **51**, 1496.
31. Kunimura, M., Sakamoto, S., and Yamaguchi, K. (2002) *Org. Lett.*, **4**, 347.
32. Nakatani, K., Hagihara, S., Sando, S., Sakamoto, S., Yamaguchi, K., Maesawa, C., and Saito, I. (2003) *J. Am. Chem. Soc.*, **125**, 662.
33. Yamaguchi, K. (2003) *J. Mass Spectrom.*, **38**, 473.
34. Sakamoto, S. and Yamaguchi, K. (2003) *Angew. Chem. Int. Ed. Engl.*, **42**, 905.
35. (a) Jeannin, Y., and Martin-Frére, J. (1979) *Inorg. Chem.*, **18**, 3010; (b) Ozawa, Y., and Sasaki, Y. (1987) *Chem. Lett.*, **185**, 923. (c) Rodewald, D., and Jeannin, Y. (1999) *C. R. Acad. Sci. Ser. IIc: Chim.*, **2**, 161.
36. Song, Y.-F., Long, D. -L., Kelly, S.E., and Cronin, L. (2008) *Inorg. Chem.*, **47**, 9137.
37. (a) Long, D.-L., Abbas, H., Kögerler, P., and Cronin, L. (2005) *Angew. Chem. Int. Ed.*, **44**, 3415; (b) Yan, J., Long, D.-L., Miras, H.N., and Cronin, L. (2010) *Inorg. Chem.*, **49**, 1819.
38. Long, D.-L., Song, Y.-F., Wilson, E.F., Kögerler, P., Guo, S.-X., Bond, A.M., Hargreaves, J.S.J., and Cronin, L. (2008) *Angew. Chem. Int. Ed.*, **47**, 4384.
39. Long, D.-L., Kögerler, P., Parenty, A.D.C., Fielden, J., and Cronin, L. (2006) *Angew. Chem. Int. Ed.*, **45**, 4798.
40. Pradeep, C.P., Long, D.-L., Newton, G.N., Song, Y.-F., and Cronin, L. (2008) *Angew. Chem. Int. Ed.*, **23**, 4388.
41. Zheng, S.T., Chen, Y.M., Zhang, J., Xu, J.Q., and Yang, G.Y. (2006) *Eur. J. Inorg. Chem.*, **2**, 397.
42. Abbas, H., Pickering, A.L., Long, D.-L., Kögerler, P., and Cronin, L. (2005) *Chem. Eur. J.*, **4**, 1071.
43. Wilson, E.F., Abbas, H., Duncombe, B.J., Streb, C., Long, D.-L., and Cronin, L. (2008) *J. Am. Chem. Soc.*, **130**, 13876.
44. Gatehouse, B.M. and Leverett, P. (1976) *J. Chem. Soc. Dalton Trans.*, 1316.
45. Marcoux, P.R., Hasenknopf, B., Vaissermann, J., and Gouzerh, P. (2003) *Eur. J. Inorg. Chem.*, **13**, 2406.

46. Wilson, E.F., Miras, H.N., Rosnes, M.H., and Cronin, L. (2011) *Angew. Chem. Int. Ed.*, **50**, 3720.

47. (a) Gun, J., Modestov, A., Lev, O., Saurenx, D., Vorotyntsev, M.A., and Poli, R. (2003) *Eur. J. Inorg. Chem.*, **3**, 482; (b) Sahureka, F., Burns, R.C., and von Nagy-Felsobuki, E.I. (2002) *Inorg. Chim. Acta*, **332**, 7.

48. (a) Cooper, G.J.T., Newton, G.N., Kögerler, P., Long, D.-L., Engelhardt, L., Luban, M., and Cronin, L. (2007) *Angew. Chem. Int. Ed*, **46**, 1340; (b) Newton, G.N., Cooper, G.J.T., Kögerler, P., Long, D.-L., and Cronin, L. (2008) *J. Am. Chem. Soc*, **130**, 790.

49. Rancan, M., Newton, G.N., Muryn, C.A., Pritchard, R.G., Timco, G.A., Cronin, L., and Winpenny, R.E.P. (2008) *Chem. Commun.*, 1560.

50. Kitson, P.J., Song, Y.-F., Gamez, P., de Hoog, P., Long, D.-L., Parenty, A.D.C., Reedijk, J., and Cronin, L. (2008) *Inorg. Chem.*, **47**, 1883.